Three-Dimensional Database of Subcortical Electrophysiology for Image-Guided Stereotactic Functional Neurosurgery

Kirk W. Finnis*, Yves P. Starreveld, Andrew G. Parrent, Abbas F. Sadikot, and Terry M. Peters

***Abstract*—We present a method of constructing a database of intraoperatively observed human subcortical electrophysiology. In this approach, patient electrophysiological data are standardized using a multiparameter coding system, annotated to their respective magnetic resonance images (MRIs), and nonlinearly registered to a high-resolution MRI reference brain. Once registered, we are able to demonstrate clustering of like interpatient physiologic responses within the thalamus, globus pallidus, subthalamic nucleus, and adjacent structures. These data may in turn be registered to a three-dimensional patient MRI within our image-guided visualization program enabling prior to surgery the delineation of surgical targets, anatomy with high probability of containing specific cell types, and functional borders. The functional data were obtained from 88 patients (106 procedures) via microelectrode recording and electrical stimulation performed during stereotactic neurosurgery at the London Health Sciences Centre. Advantages of this method include the use of nonlinear registration to accommodate for interpatient anatomical variability and the avoidance of digitized versions of printed atlases of anatomy as a common database coordinate system. The resulting database is expandable, easily searched using a graphical user interface, and provides a visual representation of functional organization within the deep brain.**

***Index Terms*—Brain atlas, electrophysiological database, Parkinson's Disease, stereotactic functional neurosurgery.**

I. Introduction

A. Problem Definition

OVER the past 30 years, image-guided neurosurgery has matured into a procedure that now sees regular use in the operating room. While many procedures are performed solely on the basis of information in anatomical magnetic resonance (MR) or computed tomography (CT) images alone, others require the incorporation of additional information that must be obtained from other sources. These additional data generally relate to the functional, rather than the anatomical structure of the brain. Functional data can be obtained from functional MR images, positron emission tomography, or from electrophysiological measurements. For example, the surgical treatment of Parkinson's Disease, essential tremor, and chronic pain entails either creating lesions or placing chronic stimulators in precise locations relative to certain electrophysiologically defined regions, deep within the brain. Planning this type of surgery involves approximate localization of surgical targets on preoperative magnetic resonance imaging (MRI) or CT images. However, neither of these modalities can delineate thalamic nuclei or functional subregions within the subthalamus or globus pallidus internus (the targets for these procedures) with sufficient contrast to enable precise direct localization.

To facilitate localization of indiscernible targets, printed anatomical atlases [1], [2] or digitized versions of them [3], [4], may be scaled to align with visible anatomical landmarks in the preoperative patient image and then displayed as an overlay. The use of individualized and population-based atlases is a major field of research in the neurosciences. A comprehensive treatment of this field is given in a book chapter by Thompson and Toga [5]. Integrating digitized atlases into computer guidance for functional neurosurgery has proven to facilitate surgical planning and, as a result, several independently developed [6], [7] and commercially available surgical planning systems have incorporated anatomical atlas-based planning modules. Registration of the atlas to the patient is typically achieved using linear scaling techniques based primarily on the length of the anterior commissural–posterior commissural (AC–PC) line and the width of the third ventricle [6], [8]. Some research oriented systems also incorporate automatic nonlinear registration algorithms for this task [7], [9]. When single or tri-planar views of a digitized atlas registered to a patient image are displayed within a surgical planning system, virtual probe trajectories that directly intersect an atlas-predicted target may be modeled prior to surgery and the stereotactic coordinates of the target region provided to the surgeon. There are, however, several limitations with existing anatomical atlases and atlas-based planning that should be addressed.

B. Atlas Limitations

Classical atlases of the human brain used in stereotactic guidance are typically derived from either one whole-brain

Manuscript received September 26, 2000; revised July 26, 2002. This work was supported in part by the Canadian Institute for Health Research under Grant MT-11540 and Grant GR-14973 and in part by a grant from the Institute for Robotics and Intelligent Systems. The Associate Editor responsible for coordinating the review of this paper and recommending its publication was S. Pizer. *Asterisk indicates corresponding author.*

*K. W. Finnis is with the Robarts Research Institute, University Hospital, University of Western Ontario, London, ON, N6A 5K8, Canada (e-mail: kfinnis@imaging.robarts.ca).

Y. P. Starreveld is with the Robarts Research Institute and the Department of Neurosurgery, University Hospital, University of Western Ontario, London, ON, N6A 5A5, Canada.

A. G. Parrent is with the Department of Neurosurgery, University Hospital, University of Western Ontario, London, ON, N6A 5K8, Canada.

A. F. Sadikot is with the Department of Neurosurgery, Montréal Neurological Institute and Hospital, Montréal, QC, H3A 2B4 Canada.

T. M. Peters is with the Robarts Research Institute and the Department of Medical Biophysics, University of Western Ontario, London, ON, N6A 5K8, Canada.

Digital Object Identifier 10.1109/TMI.2002.806567

specimen [10] or multiple hemispheres [1] from different individuals. Atlases derived from one cadaver brain are limited to only one sectioning plane per hemisphere. Those constructed from multiple subject brain hemispheres display noncontiguous anatomy in intersecting orthogonal slices when registered in an image-guidance system. With both atlas types, morphometric data pertaining to normal variations in shape, size, and position of subcortical anatomy within three-dimensions as a function of age, sex, or other factors are not available. Thus, the anatomy displayed can only be considered representative of the cadaver brains from which they were made and not the general population. The effects of normal anatomical variability are quite clearly demonstrated by the considerable mismatch that exists when digitized versions of these atlases are registered to patient images using the standard intercommissural AC–PC reference system. Registration quality within homogeneous appearing anatomy like the thalamus, where no anatomical landmarks exist, must be questioned when other discernable anatomical borders are so obviously misregistered. Some atlases [2], [11] address anatomical variability through a statistical approach but have not gained clinical acceptance for preoperative planning or intraoperative surgical guidance.

When stereotactic atlases are constructed, it is not uncommon that several cadaver tissue sections are damaged in the slicing process, sectioned unevenly, or rendered unusable by excessive or uneven shrinkage during histological processing [12]. As a result, uneven interslice distances often exist in the final printed atlas. Accordingly, during surgical planning the surgeon must frequently select an atlas plate that most closely approximates the region of brain they wish to target because there is no atlas slice that corresponds directly to the target region. When an exploratory trajectory must be translated laterally or medially within the patient's brain or inserted at an orientation oblique to the atlas plate, the nearest atlas slice available may be representative of areas several millimeters from the target. This problem is of particular relevance to the most popular of all the stereotactic atlases, the Schaltenbrand Wahren atlas [1], which contains uneven interslice distances between 1 and 4 mm. To overcome this difficulty, various investigators have scanned and interpolated one of the Schaltenbrand atlas slice series into a three-dimensional (3-D) volume [13] or have resliced it at regular intervals [14]. However, the irregular interslice distances make extensive manipulation of the data necessary to fill in the missing slices in the serial two-dimensional (2-D) volume. As a result, the anatomy contained within the volumetric atlas no longer reflects the original data.

C. Electrophysiological Confirmation

Due to the limitations described above, superposition of digitized anatomical atlases over patient brain images can provide only an approximation of target loci regardless of the atlas-to-patient registration technique employed. To refine the atlas-approximated target into a final target, multiple exploratory trajectories with a recording and/or stimulating electrode are performed within and adjacent to the intended target to characterize tissue function and to map somatotopy. Physical responses elicited by the patient, verbal descriptions of stimulation induced phenomena, and microelectrode recording (MER) data obtained during exploration help the surgeon to mentally reconstruct the somatotopic organization contained within the target structure and to establish functional borders. Comparison of the patient somatotopic organization with that contained in the literature allows estimation of probe tip position within the target and is used to plan subsequent trajectories until the ideal target loci are determined.

The electrophysiologically refined target, as shown in studies focusing on pallidotomy [15], [16] (lesioning of the globus pallidus internus) and chronic subthalamic stimulation [17], [18], can be shifted dramatically from the original atlas-derived or visually identified stereotactic target once electrophysiological exploration was performed. These studies demonstrated that targeting using standard techniques often results in poor initial targeting accuracy.

D. Electrophysiological Databases

In attempts to increase initial targeting accuracy of the surgical target, numerous authors have compiled and analyzed functional information from subcortical structures from many individuals acquired during stereotaxy [19]–[22]. The electrophysiologic data were standardized using alphanumeric codes and normalized to an anatomical atlas, to create composite functional maps. Registering electroanatomic observations from a series of patients to a common coordinate space made examination of functional organization in relation to anatomic structures possible. Bertrand *et al.* [23] first introduced this technique when they displayed a crude somatotopic organization of corticobulbar and corticospinal fibers within the posterior limb of the internal capsule, derived from a population of 26 patients normalized to a representative slice of the Schaltenbrand Bailey [24] atlas. They later augmented this technique [19] to include interactive recording and display of physiologic responses obtained during surgery. In 1982, Tasker *et al.* [20] published the microstimulation results of 9383 sites during 198 procedures, primarily for Parkinson's disease and chronic pain. Tasker's work represents the most comprehensive analysis of electrophysiologic observations obtained through microstimulation available to date.

Current electrophysiological atlases do provide an approximation of functional organization within some subcortical structures, but are of limited use as a source of surgical guidance. The poor clustering of population data results primarily from the inability of linear registration to accommodate interpatient anatomical variability. Also partially responsible is the practice of plotting inherently 3-D data on a 2-D atlas that exhibits irregular interslice distances. This necessitates patient data being mapped to fit the atlas slice considered most representative of the volume of brain being explored adding an additional 2- to 3-mm localization error to that incurred by the use of a linear registration process. Further, the coding schemes typically employed are not sufficiently flexible to describe all aspects of an observed response in relation to the parameters that evoked it or the characteristics of the patient from whom the data originated. Despite their limitations, the early electrophysiologic atlases form an excellent foundation for the work described in this paper.

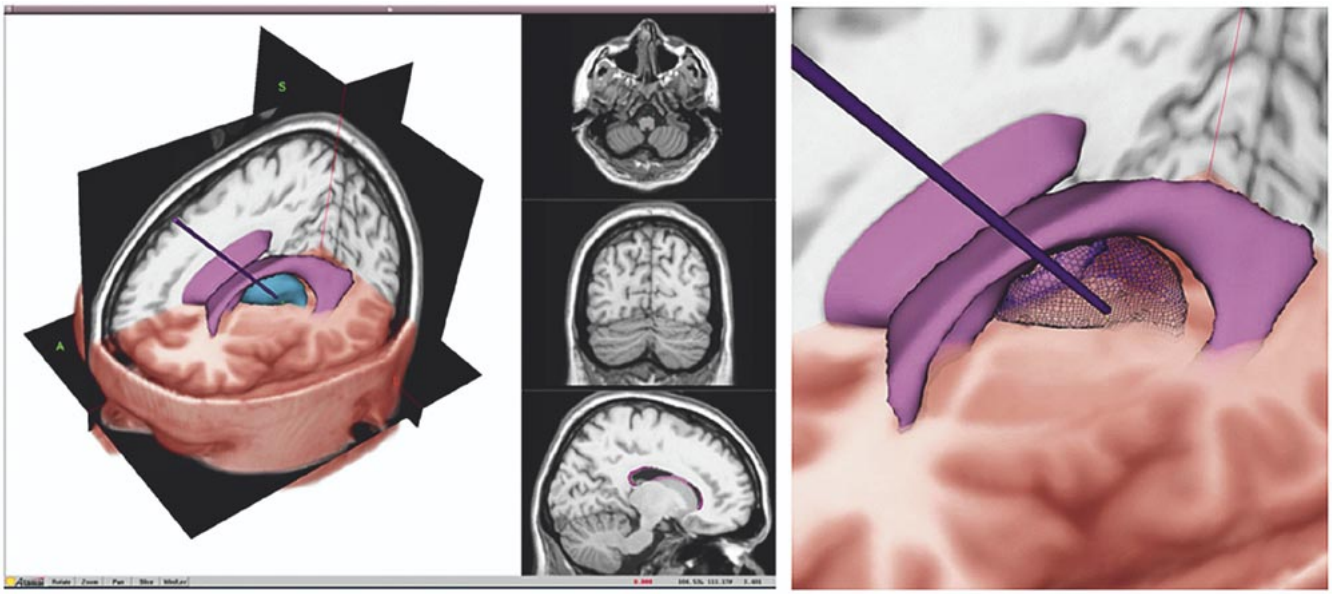

Fig. 1. (left) One of many possible display configurations of the ASP visualization platform. Three orthogonal views of a T1-weighted MRI are shown on the right of this image. Larger window displays intersecting orthogonal MRI planes with surface rendered ventricles (purple) and left thalamus (blue). A partial volume rendering of the MR image is simultaneously displayed. An exploratory electrode is shown intersecting the lateral aspect of the thalamus. (right) Magnification of region around the left thalamus, ventricles, and modeled electrode. Thalamus displayed as a triangulated mesh.

E. Electrophysiological Database

We describe below a computerized 3-D database of deep-brain electrophysiology containing functional data from 106 procedures performed on 88 patients at the London Health Sciences Centre (LHSC). Our approach incorporates several advantages over standard techniques: 1) addition of electrophysiologic data to the database does not rely upon AC–PC-based global or piecewise linear registration or manual identification of anatomical landmarks; 2) a high signal-to-noise reference MR image is used as the common coordinate system for the database rather than a series of digitized anatomical atlas slices; 3) accommodation for anatomical variability is achieved using a nonlinear registration algorithm that "warps" the deep brain anatomy as observed in a patient MRI to that of the reference MRI; 4) a comprehensive coding protocol for describing observed responses is coupled to an interactive graphical user interface (GUI) for ease of use; 5) database codes are easily accessible through a flexible search engine that permits searches of varying specificity; 6) search results may be displayed as autonomous 3-D objects or as cluster probability maps that can be nonlinearly registered to the MR images of individual patients; and 7) these features are integrated into a visualization software package capable of planning and guiding a functional stereotactic procedure from start to finish.

II. Methods

A. Visualization Platform

We have developed a new visualization and development environment, Atamai Surgical Planner (ASP)[1] [25], to record and display functional data and to enable rapid prototyping and implementation of many image-guided surgery applications in our laboratory. ASP can register and fuse data from MRI, magnetic resonance angiography (MRA), CT, ultrasound, video and physiological recordings, and interface with a variety of tracking systems for intraoperative registration and guidance. This visualization platform was written using VTK (the Visualization Toolkit, Kitware, Clifton Park, NY, http://www.kitware.com) and Python (http://www.python.org) making it both operating system and hardware platform independent. In addition, the system is capable of interactively displaying stereoscopic 3-D image data, comprising texture-mapped, surface and volume-rendered data (Fig. 1).

The primary interface consists of three intersecting orthogonal planes (axial, coronal, and sagittal) that may be moved through the volume independently and re-sliced obliquely. Functional data-points extracted from the database are displayed as individual spheres whose centroids are positioned at their associated 3-D image–space coordinates. For responses obtained by microstimulation, the magnitude of the current employed to evoke the response is used to scale the diameter of the representative sphere according to a metaanalysis performed by Ranck [26] for exciting specific volumes of an average of gray and white matter within mammalian brain using a monopolar electrode with pulse duration normalized at 0.2 ms at 300 Hz. This scaling factor is provided as an approximation of the probabilistic spatial extent of the neuronal pool involved when a response was evoked, but should not be interpreted as an absolute measure.

B. Image Registration

There are two image-registration steps required to successfully implement our objective. The first is the rigid-body registration step necessary to register the image with the patient, whereas the second is required to perform the nonlinear mapping of the recorded data to the database, as well as to apply the database to an individual patient.

[1]Available: www.atamai.com.

1) Patient-to-Image Registration: We have developed an automatic fiducial localization algorithm (the "Frame-finder") [25], [28] that scans through every axial slice within a patient MRI volume, extracts the Leksell stereotactic frame fiducials, and computes a volume-based image–space to frame–space registration transformation.

The algorithm first computes the average intensity of all voxels within the image and then thresholds the volume in order that only those voxels with intensity values three standard deviations above the global image mean are further considered. This cutoff robustly identifies the high signal levels from the fiducials seen on T1, T2, and proton-density images. The remaining pixels in each axial image are searched for clusters containing a sufficient number of contiguous voxels that would correspond to the known cross-sectional area of the fiducials.

A linear least squares fit is computed for each bar identified in this manner, with outlier points being iteratively removed to reduce the sensitivity of the algorithm to local distortions in the magnetic field. For each fiducial plate, the intersections of the diagonal bar with each of the two vertical bars are computed, and the coordinates of the free ends of the vertical bars calculated from their known length. This step generates four landmark points for each of the left and right fiducial plates. These points are then used to compute the rigid body transformation matrix that transforms there image space coordinates, to the known Leksell frame coordinates of these same locations. Unlike most frame-coordinate localization procedures, this approach computes the best fit, at a subvoxel level, of a frame to its representation in the MR volume and is robust to local distortions in the MR frame image.

We tested this algorithm on a 3-D frame-mounted phantom with targets distributed uniformly within a 200 mm^3volume, and whose positions were identified using the stereotactic frame pointer. Image-based calculations of these coordinates demonstrated a mean localization error of 0.5 ± 0.3 mm for CT and 0.6 ± 0.3 mm for MRI [25]. In addition, in order to verify its robustness on clinical data, we verified by visual inspection that the algorithm could correctly locate the fiducials on 175 typical preoperative stereotactic MR image volumes ($256 \times 256 \times 248$ voxels, 160 patients) acquired with the Leksell frame fixed to the patient. Computation time was less than 1.5 s/image volume on a personal computer (1-GHz Pentium III).

2) Data-to-Database and Database-to-Patient Registration: This step requires a nonlinear registration procedure. We originally employed a previously validated [27] nonlinear registration algorithm, "ANIMAL" [9], to nonlinearly register (warp) the patient's preoperative image and functional data to a standard, high resolution MRI reference brain. Unfortunately, using this algorithm the length of time required to warp a patient brain to the target MRI, at a scale of 2 mm, was in the order of 8 hours, which limited its applicability for the task. However, we have recently begun to use a new rapid warping procedure, implemented in Vtk and Python, which can compute the warp in less than 10 min on a 1-GHz P III computer [28].

The nonlinear registration methodology is comprised of two separate components. The first generates a global affine transformation that maximizes the normalized cross-correlation between the source and target volumes. In addition, an arbitrary closed polygonal model enveloping different aspects of the image may be selected to act as a mask to constrain the search-space for the similarity measurement. Masking permits the user to bias the optimization of the affine transform so that specific regions, such as the diencephalon, may be brought into better registration at the expense of extra-cranial or cortical structures. The second step builds upon the affine registration by computing a deformation grid that maximizes the similarity metric on successively smaller subvolumes of the images. While a complete description of this algorithm is contained in [28], the essential steps in this algorithm are presented in Fig. 2.

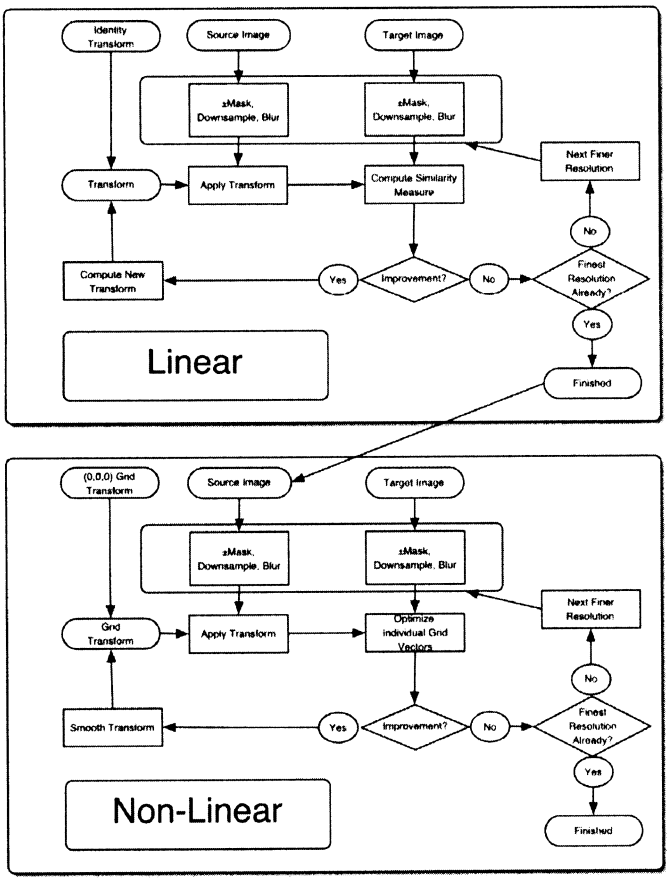

Fig. 2. Flow chart outlining the principal steps incorporated into the linear and nonlinear registration algorithms.

The Python/Vtk implementation of this algorithm has been parallelized, allowing us to further reduce the computation time by distributing the cubes to be aligned over the number of processors available.

3) Assessment of Nonlinear Registration: Objective validation of nonlinear warping in a clinical context is a difficult problem. Simple subtraction of images is dependent on relative intensities of source and target and even when perfectly registered, subtraction may not obviously demonstrate this fact. We use a feature of the warping algorithm itself to assist in the assessment of the registration. The warping algorithm we have described maximizes the normalized local cross correlation values of two images by computing a field of deformation vectors that optimally align the local domains of one image to another. Computing the normalized cross correlation for each domain across the entire image volume provides a three

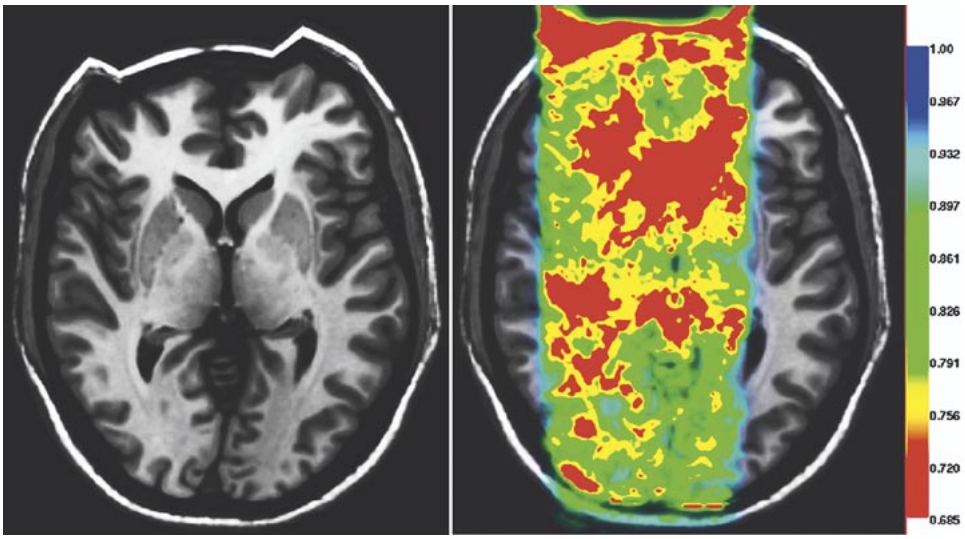

Fig. 3. (left) A T1-weighted brain volume distorted with a deformation grid that progressively shifts the middle third of the volume posteriorly as one moves anteriorly in the image. The maximum displacement is 16 mm. (right) A normalized cross-correlation map, computed based on the left image and its original undistorted version. Map is displayed superimposed on the distorted image and linked to color-coded scalar bar. Red indicates lowest average correlation.

dimensional volume of cross-correlation values. However, this metric is only sensitive to the scale at which it is computed. If the size of each domain is a 2-mm cube, then a misregistration occurring at a larger scale will only manifest itself as a narrow strip of low normalized cross-correlation values. In order to be sensitive to misregistrations at all relevant scales, we compute a series of the normalized cross-correlation map using domains consisting of cubes of 16, 8, 4, and 2 mm. The larger scale maps are then subsampled to 2-mm spacing and all are averaged together to provide a single composite map. This approach differs from image subtraction as a measure of the degree of alignment in that it is insensitive to variations in image intensity.

This map can be displayed registered to the target image to provide a rapid visual check of registration quality as a function of position within the image volume. One can assess the quality of the registration of individual structures of interest, by sampling the map at the locations contained in that structure. A demonstration of the cross correlation map is presented in Fig. 3. Fig. 3 (left) displays a T1-weighted image deformed using a grid that progressively shifts the middle third of the image volume posteriorly as one moves anteriorly in the volume. Using this grid, minimal shift is produced in the occipital cortical region while a maximum displacement of 16 mm is achieved in the frontal lobes and forehead. A cross correlation map was computed based on the deformed and nondeformed image volumes and is shown superimposed on the deformed image [Fig. 3 (right)]. The regions with lowest averaged correlation appear in red while those with greatest correlation appear in shades of blue. Perfect correlation (darkest blue) was made transparent in this map.

Because this algorithm is driven by gradients in the image, homogeneous regions surrounded by edges do not generate deformation vectors. To overcome this difficulty, within such regions the algorithm interpolates new vectors that are a linearly weighted combination of the surrounding vectors.

4) Standard Brain Image: Due to its extensive use in the neuroscience community as a standard brain template, to date we have used the standard CJH-27 brain template [29] as the target MRI brain image. CJH-27 consists of 27 registered T1-weighted MRI scans of the same individual averaged into a single volume and provides a high signal-to-noise ratio image volume as the common image space for all functional data in the database.

While the CJH-27 brain has seen extensive use in many centers as a standard brain image template, it is not necessarily representative of the population of patients in our study. However, now that we have access to a rapid image-warping algorithm, we are in the process of developing a new average MRI brain that will be more representative of the patient population in the study. We will employ the methodology recently described by Kochunov *et al.* [30] to select, from a specific patient population, a target reference brain that is most representative of that population, in the sense that it is the sample from the population that would require the minimum deformation of the rest of the members of the population to match it.

Each 3-D patient image acquired for surgery planning is nonlinearly registered to this standard brain. The 3-D grid describing this warp that is produced for each patient volume is then used to re-map coordinates of their coded electrophysiologic data from patient native image–space to the image–space of the standard brain. The inverse of the deformation matrix generated as part of this procedure can then be employed to directly map points in the population-based electrophysiology database to the anatomy of the individual brain, avoiding the use of the linear atlas registration techniques commonly employed.

C. Patient Selection and Imaging

Patient data entered into the database were selected from a population operated on for the treatment of Parkinson's disease,

essential tremor, and chronic pain at the LHSC. The Leksell G stereotactic head frame (Elekta Instruments AB, Stockholm, Sweden) was used in each procedure. All patients were retrospectively selected for database inclusion based on the clarity and detail of their intraoperative notes or dictations and the existence of their archived T1-weighted MR image.

Excluded from the study were patients exhibiting prior stereotactic lesions, space occupying brain masses or pathology that might distort somatotopy or compromise the nonlinear warping procedure. A 1.5T GE Signa MR Scanner using a 3-D SPGR sequence with TR: 8.9 ms, TE: 1.9 ms, $Nex = 2$ and flip angle of 20° was used to produce a 1.17 mm $\times$ 1.17 mm $\times$ 1 mm (out of plane) resolution volume for each patient. We have also collected and entered data from a second site (the Montreal Neurological Institute—MNI), but since historically most of these procedures used somewhat different stimulation/recording and reporting methods compared with those reported above, a selective search with respect to physician and/or data origin allows us to select only data acquired at the LHSC. MNI data have, therefore, not been included in the examples presented here. As more patients from this site and others are collected and processed using a standard methodology (the ASP platform), such data will be able to be fully included in all studies.

D. Surgical Procedure

Surgical targets were chosen based on the nature of the disease. The Ventralis intermedius (Vim) nucleus of the thalamus was targeted for tremor dominant diseases, the Ventralis caudalis (Vc) nucleus of the thalamus for chronic pain, and the globus pallidus internus or subthalamic nucleus (STN) for Parkinsonism. For each procedure, between two and nine trajectories were used to refine the approximated target into a final one. Patients were awake, and whenever possible not medicated, at time of surgery.

1) Indirect Targeting: Standard practice for identifying the best "initial-guess" targets involves MRI console-based planning on a single axial image thought to contain the target. The approximated target is identified on this image through AC–PC scaling of anatomical atlas-based coordinates to match the intercommissural distance of the patient. Diagonally joining the anterior to posterior fiducials of the opposite lateral plates on an axial image and locating the intersection of the lines determine the geometric center of the frame. Stereotactic coordinates are assigned to the target relative to the frame center. It is important to note that this manual procedure for identifying the frame coordinates of the initial target from the MR console provides only the estimate of the coordinates of the initial exploratory trajectory. Since the coordinates of all recordings are read directly from the stereotactic frame, inaccuracies in this initial estimate have no effect on the overall accuracy of the process.

2) Neurophysiological Target Verification: Surgeons at the LHSC use a combination of MERand electrical stimulation to map the functional characteristics of the deep brain. For each trajectory, a tungsten microelectrode capable of recording neuronal activity or applying electrical current was advanced from 10 mm above the target anatomy to 5 mm below using a custom built microdrive. During MER, a simultaneous audio and oscilloscope system is used to visualize and listen to neuronal spike trains in real-time. Electrode tip positions are noted each time neuronal activity was encountered that could be correlated to a receptive field on the patient's body. Following MER exploration, microstimulation is typically applied using currents ranging from 5 to 120 μA (300–Hz, 0.2–ms pulse duration). Depending on the region of brain being explored, supra-threshold stimulation commonly evokes visual phenomena, muscle contractions, or cutaneous sensory responses through involvement of the optic tract, corticospinal tract, and somesthetic pathways, respectively.

Once the functional organization of the target anatomy is mapped and an ideal locus determined, a series of radiofrequency lesions are made or a chronic stimulator electrode is implanted at the target. All patients received a postoperative MRI one day following the procedure.

E. Standardizing Electrophysiologic Data in Patient Native MRI-Space

All stimulation-induced responses and MER data are quantified and standardized using a six-parameter code before being entered into the database. This code contains the following information: 1) A patient identification number; 2) A trajectory identification number; 3) Data acquisition method (including recording and stimulation parameters); 4) Laterality of response; 5) A body part number assigned to a discrete region of the body; and 6) A response code describing the quality of the response or changes in cell firing patterns.

For parameter five, a subdivided model loosely based on Tasker's version [20] of the Woolsey figurine for physiologic data recording was designed and integrated into an interactive GUI (see Fig. 4). Each anatomical subdivision and groups of subdivisions on the homunculus model were assigned unique identification numbers that can be selected by the user for anatomically localizing each response. For parameter six, 80 response descriptors were created using a hierarchically organized user interface that allows rapid assignment of the appropriate standardized code to any given response. The user may also append text to the chosen response code to qualitatively describe the observed response.

This coding method was implemented in such a way that an experienced user could readily determine important data linked to each response through inspection of the code. The multiparameter nature of each code made it possible for us to design a highly flexible database search engine, written in Python, that extracts and displays database codes matching any field or combination of fields specified by the user.

Within our image-guided neurosurgery system, coded functional data are plotted directly onto the patient's preoperative image along a virtual trajectory that corresponded to the position and orientation of the physical probe. Images are registered to the coordinate system defined by the stereotactic head frame using the Frame Finder software algorithm incorporated into the visualization platform. The image-to-frame transformation generated by this algorithm allows us to display the functional data codes on the appropriate anatomical area of the image in 3-D space.

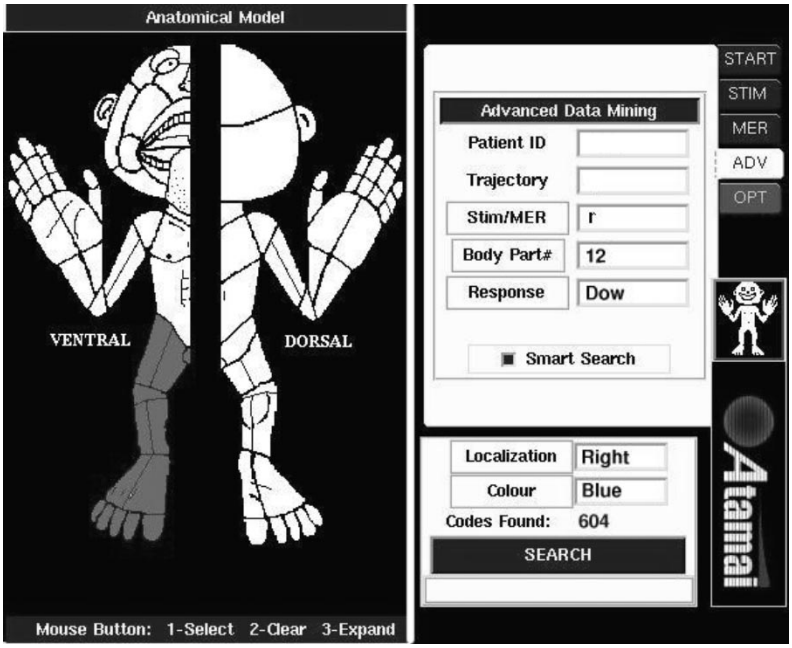

Fig. 4. Graphical user interface used to enter new data in patient image–space and for searching database contents. The user may indicate the receptive/projected field for any response on the interactive homunculus model on the left. Ventral surface of the leg and foot are shown selected here.

Once annotated to their respective imaging volumes, the Cartesian coordinates of the patient-specific functional data, along with their corresponding codes, are saved in a text file for addition to the central database. A secondary code describing the sex, age, pathological condition, and handedness of the patient, surgical procedure and specifications of the probes used during the procedure is assigned to the header of each data file. When patient functional data are fully coded and annotated to their respective MRIs, the image and functional data are nonlinearly registered to the common image space of the central database.

III. Application of Method

The database currently contains over 10 000 individually coded data-points provided by 88 patients (106 procedures). Until now, all electrophysiological data have been entered into the database retrospectively, but we are nevertheless in a position to demonstrate the effectiveness of this system in displaying functional organization of basal ganglia structures. Only those data obtained from the LHSC site are presented in the following figures.

A. Representative Database Searches

1) Motor Thalamus: Fig. 5 demonstrates a probabilistic functional border between two nuclei of the left thalamus, the Vim motor nucleus and the Vc sensory nucleus described above. Individual purple spheres (diameter = 0.2 mm) represent data encoding for kinesthetic neurons (neurons detected using MER whose activity may be activated or inhibited by specific movements around a joint). Green spheres represent tactile neurons discovered during MER when light touch of a specific region of the patient's body induced neuronal excitation. While moderate overlap exists between the two regions (as one would expect) there is an obvious transition between the population-based motor and tactile regions. The tactile neuronal cluster may be further subdivided to reveal a medial-to-lateral somatotopic organization similar to that revealed in the previous figure. The somatotopy within the population Vim data is less distinctive, however, a jaw-medial to foot-lateral organization is present (not shown). The anterosuperior orientation of the cluster distribution seen in this figure is indicative of the frontal burr-hole approach used during thalamotomy, defining the typical trajectories to reach this region.

2) Sensory Thalamus: The Vc nucleus is a sensory nucleus found within the posteroventral aspect of the thalamus and thought to be somatotopically organized. During thalamotomy (therapeutic lesioning of the thalamus) for Parkinson's Disease, essential tremor, and chronic pain, the functional organization of this nucleus is extensively mapped using the electrophysiological exploration techniques described above, and its functional borders determined. Fig. 6. presents the results of a selective search of the database for sensory responses characteristic of those obtained during Vc microstimulation at less than 100 μA and 300 Hz. Note the presence of somatotopic organization occurring naturally within these population data.

3) Subthalamic Nucleus (STN): Over the past ten years, the STN has received increasing attention as a surgical target for treating Parkinson's Disease and other movement disorders. This is due, in part, to the evidence that decreasing STN hyperactivity by chronic deep brain stimulation (dbs) may slow or halt progression of the disease by removing potentially excitotoxic effects [31]. The STN, although partially visible with T2-weighted or fast spin echo inversion recovery MRI sequences, must still be electrophysiologically defined to minimize stimulation effects on surrounding structures (such as the internal capsule, medial lemniscus, ventral thalamic nuclei,

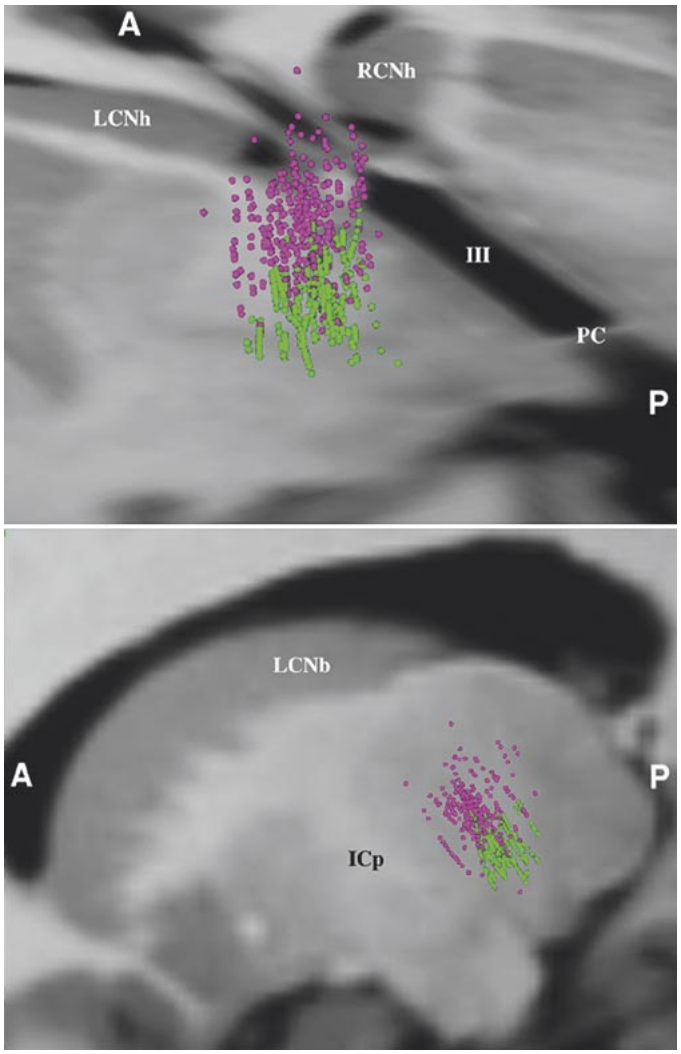

Fig. 5. Probabilistic functional border between two left thalamic nuclei, the Vim motor nucleus and Vc sensory nucleus, in reference brain image–space. Each sphere indicates where a microelectrode encountered neurons either kinesthetic in function (purple spheres—representative of the Vim nucleus) or tactile in function (green spheres—representative of the Vc nucleus). *Top*: Oblique view of axial plane at level of posterior commissure. Data are clustered just above the image plane. *Bottom*: Sagittal view. 929 data points collected from 26 patients. *A: anterior, P: posterior, III: third ventricle, PC: posterior commissure, LCNh/RCNh: left and right head of the caudate nuclei, LCNb/RCNb: left and right body of the caudate nuclei, ICp: posterior limb of the internal capsule.*

and substantia nigra) by the dbs electrode [32]. We demonstrate in Fig. 7 how the database may ultimately be used to aid placement of dbs electrodes. The 3-D model of a typical quadripolar dbs electrode faithfully displays the position and dimensions of the exposed contacts. The user may modify the visualization parameters to reflect the configuration of their institution's dbs electrodes. Yellow spheres represent 27 separate locations where multiunit recording detected tremor-synchronous neuronal activity, magenta spheres indicate where neurons with activity characteristic of the STN were found but could not be localized to a particular receptive field, and cyan spheres indicate neurons considered kinesthetic in function. The larger red spheres intersecting the axial plane represent paresthesias evoked during exploratory electrical stimulation.

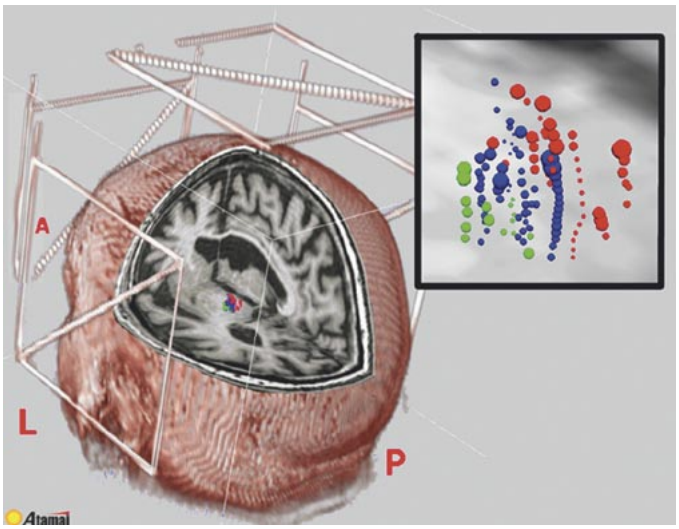

Fig. 6. Posterior view of a volume rendered patient preoperative MRI scan. Cutaway reveals cluster of data extracted from the database following nonlinear registration to this imaging volume. The fiducial bars are visible surrounding the patient's head. (inset) Magnification of data extracted from the database encoding for paresthetic responses characteristic of the Vc sensory nucleus. All responses were evoked using microstimulation with less than 100-μA current at 300 Hz. Note the medial to lateral somatotopic organization of these population data (face medial to foot lateral): Red—Paresthesias of the mouth and tongue. Blue—Paresthesias of the contralateral fingers. Green—Paresthesias of the contralateral foot. Data were procured from 15 patients. *P: posterior, L: left, A: anterior*.

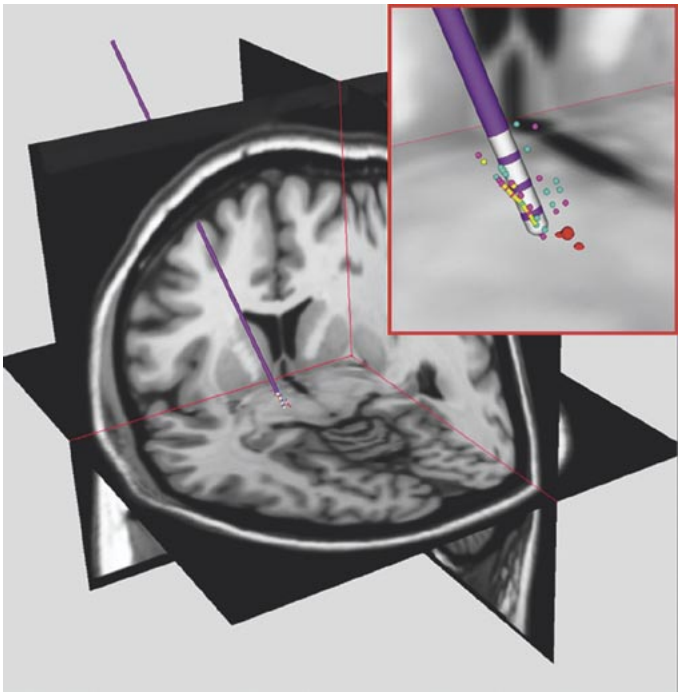

Fig. 7. Reference brain MRI and modeled quadripolar deep brain stimulator with tip inserted into left subthalamic nucleus. Inset: Results of a search for functional data characteristic of those acquired during STN procedures. Yellow spheres: tremor cells. Magenta spheres: cells with firing patterns characteristic of STN neurons (with no obvious receptive field). Cyan spheres: neurons with kinesthetic activity. Red spheres: stimulation induced paresthetic responses.

B. Data Display

With the addition of more subjects, it becomes obvious that visualization of large quantities of data must be clear and un-

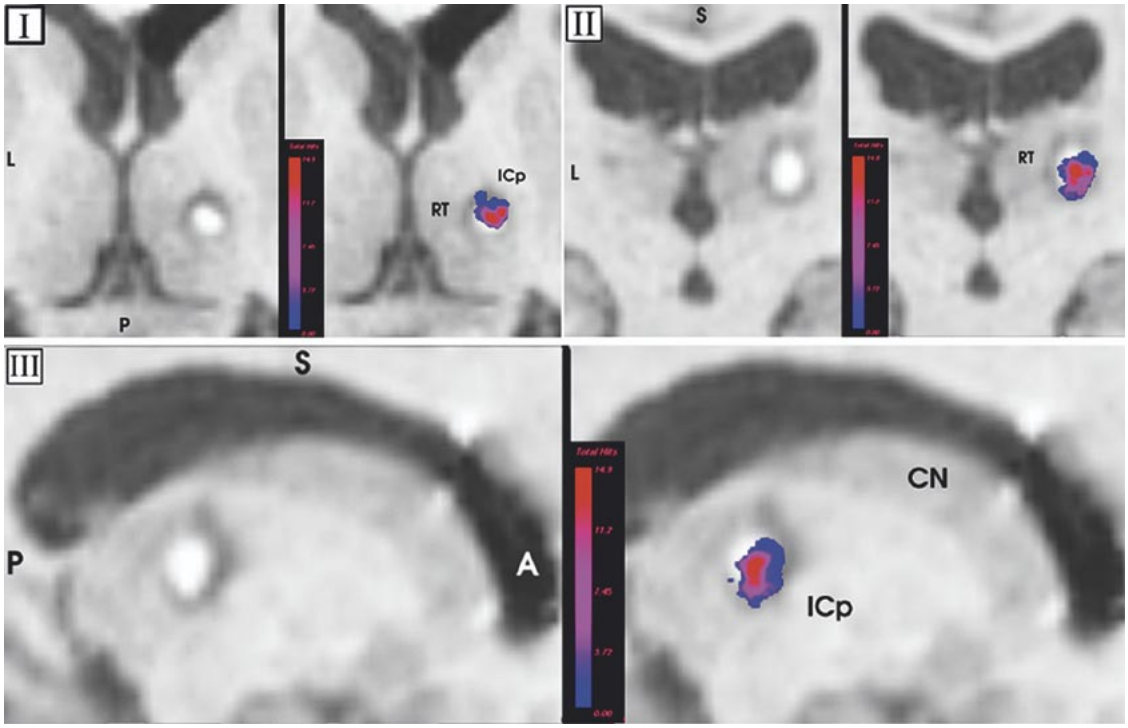

Fig. 8. Image pairs displaying a patient postoperative MRI following right thalamotomy and the same image with a density plot overlay. Density plot indicates where the greatest overlap of population data encoding for stimulation-induced tremor arrest exists once nonlinearly registered to this patient's image. Blue represents lowest likelihood of eliciting tremor arrest upon high frequency stimulation while red indicates the greatest likelihood and the strongest prediction for lesion placement. Note that the region of greatest probability lies within the hyper-intense boundary of the lesion. I: axial plane, II: coronal plane, III: sagittal plane. *A: anterior, P: posterior, S: superior, L: left, RT: right thalamus, ICp, posterior limb of internal capsule, CN: caudate nucleus*.

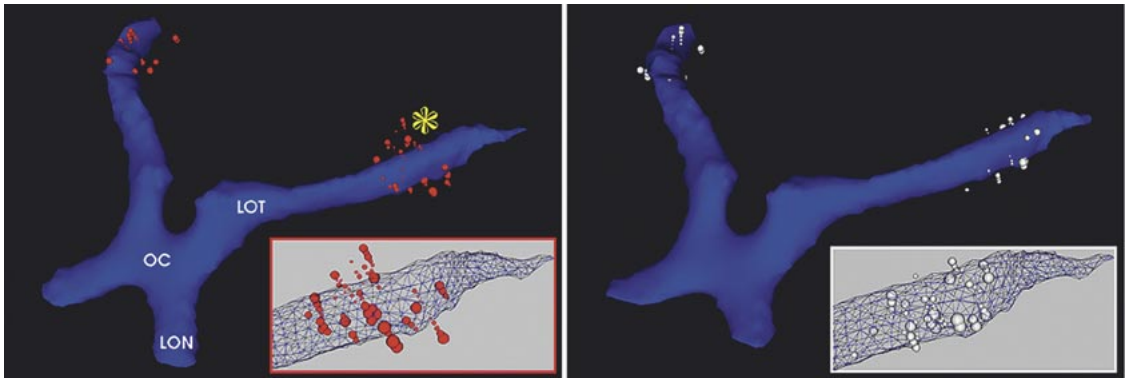

Fig. 9. Optic tracts, chiasm, and portions of the optic nerves (blue) manually segmented from the reference brain image. Spheres represent stimulation-induced flashing lights reported in the patient's visual field indicative of probe tip proximity to (or insertion within) the optic tract. Insets display magnification of the region of left optic tract situated inferior to pallidum as a triangulated mesh. (left) Red spheres represent these data in reference brain image–space after AC–PC linear registration. Yellow asterisk indicates position of the base of the globus pallidus internus. (right) Same data as in left, however, all data spheres (white) were registered to the reference image using our nonlinear registration algorithm. *LOT: left optic tract, OC: optic chiasm, LON: left optic nerve*.

ambiguous. Our primary method of data display presents each response as a single sphere with diameter determined by the method used to evoke it. While this approach has proven quite effective, it eventually taxes computer memory to an unacceptable level when many data elements are displayed. The meaning of large clusters of individual spheres can also be difficult to interpret due to overlapping and obscuring of data, but is still preferable to a 2-D display of superimposed alphanumerics.

We, therefore, developed a secondary display representation that is better suited for displaying large quantities of data. With this display mode, a transparent 3-D rectilinear grid with 0.25-mm isotropic cells is created over the deep brain region of interest. Each grid cell is initially assigned a value of zero. When functional data are extracted from the database and assigned a 3-D spherical shape with specific radii, they are superimposed over the grid but not rendered in the scene. Those grid cells overlapped by a functional data sphere have their values incremented by the fraction of the cell volume within the sphere. The remaining grid cells not in contact with the sphere remain at a zero value. The grid data are mapped to a color scale for display. When visualizing data in this manner, the user only sees the functional data currently intersecting the position of the image planes. Both display modes may, however, be used simultaneously for maximum clarity.

The regions displayed indicate areas of patient anatomy that, when explored electrophysiologically, would have a statistically higher chance of producing a specific response. The strength of prediction is dependent on the amount of data represented within the region, stimulation parameters, and how tightly the population responses cluster.

C. Lesion Correlation

Electrical stimulation during thalamotomy for tremor-dominant movement disorders can have the same outward effect as a lesion but, unlike a permanent radiofrequency lesion, has reversible effects. This property allows stimulation to be used as the final check for lesion placement through correlation of tremor modulation with the application of current. Fig. 8. presents a one day postoperative image of a patient who received a right thalamotomy for contralateral tremor. The density of responses is displayed as outlined above. The lesion appears as a hyper-intense ellipsoid region with a ring of hypo-intense edema within the lateral right thalamus. In each of the three views (axial, coronal, and sagittal), we show the results of a database search for data encoding for stimulation-induced tremor arrest. Data from ten different patients (67 discrete data points) are included in this sample. Using the display mode just described, we show a cluster density map linked with a color scalar bar that depicts regions of low cluster density (blue) to high density (red). Regions of highest cluster density and strongest database prediction are found completely within the lesion boundary. It should be noted that this patient's intraoperative data were intentionally excluded from the database sample shown in these images and that the surgical procedure was planned and performed using standard techniques, and did not take advantage of the functional atlas. Upon two-month postoperative follow-up, this patient was found to be ~95% tremor-free.

D. Clinical Validation of Nonlinear Registration Approach

Since it is difficult to identify most stereotactic targets in the MR volume on the basis of anatomy alone, objective validation of our nonlinear approach is not straightforward. However, we believe that the following example provides solid evidence of the validity of nonlinear registration in pooling electrophysiologic observations.

During pallidotomy, surgeons locate the optic tract situated just inferior to the apex of the internal pallidum by correlating patient descriptions of stimulation-evoked visual phenomena with the position of the probe tip. The optic tract acts not only as an anatomical landmark during exploration but also signifies a region of brain that must be spared during GPi lesioning or dbs insertion. A neuroanatomist (KWF) manually segmented the optic nerves, chiasm, and anterior portion of the optic tracts from the CJH-27 volume. The resulting closed 3-D polygonal surface representing these structures is displayed in blue in Fig. 9.

When the stimulator tip is situated within the optic tract of the patient during exploration, a minimum current threshold is required to evoke visual phenomena. This current threshold increases as the probe tip is moved away from the optic tract. Electrophysiological data (143 points from 26 patients) representing flashing lights in the visual field were registered to the reference brain using two different approaches. In both cases, the current magnitude required to evoke each response is indicated symbolically by sphere diameter. The first [Fig. 9 (left) red spheres] used a nine degree-of-freedom (translation, rotation, scale) linear registration to align the AC and PC landmarks between the source images and the target. Note the large spread of the data points and the displacement from the ideal region (optic tract) in the target image. A magnification of data clustering around and within the segment of the left optic tract situated just inferiorly to the base of the internal pallidum (yellow star) is provided in the insert. The segmentation in the insert is displayed as a triangulated mesh so that spheres positioned within the optic tract are visible.

Conversely, when the nonlinear procedure is used to perform the mapping [Fig. 9 (right) — white spheres], significantly more data points lie within the optic tract segmentation, the clustering of these data is considerably tighter, and the points tend to follow the tube-like geometry of the tract [Fig. 9 (inset)]. A quantitative assessment of the efficacy of this approach indicates that 71% of the data points were within or touching the optic tract after nonlinear registration, whilst only 50% of the points did so with AC–PC linear registration. In addition, of the 29% of the data points situated outside of the segmentation following nonlinear registration, the point with the greatest displacement from the polygonal surface was found 2.8 mm away and was evoked using 117-μA current. Following AC–PC registration, the point situated furthest from the segmentation surface was located 4.1 mm from the surface and was evoked using 25 μA. Intuitively, the point furthest from the anatomy of origin would require significantly higher stimulation current to achieve threshold and evoke visual phenomena than any data point lying within it. A distance-to-current relationship was evident within those points external to the segmentation following nonlinear registration but not observed in the same group following AC–PC-based registration.

In this example, all responses were evoked with a microelectrode using less than 117-μA current at 300 Hz. These data indicate that nonlinear registration clusters interpatient visual pathway data within or in very close proximity to the only anatomical structure capable of eliciting the response with abilities superior to AC–PC-based linear registration.

IV. Discussion

A. Advantages

Previously, databases of electrophysiology integrated into stereotactic planning systems have been restricted to a 2-D display and relied upon digitized atlases of anatomy to provide a common coordinate space. We have described a method and presented results for the first truly 3-D collection of subcortical electroanatomic observations capable of nonlinear registration to a patient MRI. The resulting database contains the intraoperatively derived functional data from a population of 88 patients and resides within the space of one reference brain MRI. All registrations (patient data-to-reference image

and database-to-patient) were achieved using our rapid warping algorithm to accommodate for nonlinear anatomical variability.

When database contents are selectively displayed within our visualization program, delineation of functional borders within homogeneous appearing anatomy is possible, high probability tremor areas can be identified, and somatotopic organization may be visualized.

Our interactive GUI makes generic or detailed searches possible. Using the interface, the surgeon can extract and display only those data most closely approximating their patient's age, sex, handedness, and diagnosis, or conversely choose to view only data representative of a larger cross section of the database population. For electrical stimulation-evoked responses the database may be queried for only those data produced using probe and stimulation parameters including current, voltage, frequency, pulse duration and probe diameter similar to that used by the surgeon. The interactive GUI has provided three significant advantages to this project. First, it facilitates rapid, detailed coding of patient data that will not impede the normal flow of the surgical procedure if used intraoperatively; it is sufficiently generic to allow expansion of the database to include other procedures and anatomy; and it will vastly simplify integration of surgical data from multiple institutions.

B. Caveats

This project incorporates the basic concepts of the work previously described by Thompson, Bertrand, Tasker, Yoshida and Giorgi and others [19]–[22], [33] but introduces significant increases in scope and functionality with superior visualization capabilities. We believe that our approach of consistently determining the stereotactic frame coordinates via the "frame-finder," and our nonlinear image registration method significantly reduces the extent of the errors involved in the mapping procedure. However, even with these enhancements there are sources of error inherent to every functional stereotaxy surgery that cannot be addressed by our paradigm.

The interpretation of descriptions provided by patients following stimulation or the visual and aural analysis of MER spike trains is qualitative and subjective. When a patient describes a tingling sensation of a certain body part upon stimulation, the surgeon must assume that this was exactly what the patient experienced and nothing more. During microelectrode recording within sensorimotor nuclei, patient's joints are manipulated so neuronal excitation or inhibition may be correlated with a joint and a specific movement around that joint. When a receptive field is found that modulates the firing, for example flexion of the patient's hand at the wrist, the surgeon will typically investigate other combinations of motions but can never be certain that the neuronal activity is directly correlated to that single movement and not a combination of movements or even a different part of the patient's body which may have moved unbeknownst to them. The qualitative interpretation of patient responses is dependent upon the training and experience of the operating surgeon and has formed the basis of this procedure for over 50 years. As such, we feel confident that the utility of an atlas comprised of qualitative observations will not be diminished by the somewhat subjective nature of the data.

Deflection of the microelectrode as it traverses brain tissue of varying densities may result in data being tagged at the tip of the straight virtual electrode within ASP when the site of origin was actually an unknown distance away. Although electrode deflection is minimized through the use of a cannula that guides the probe to a position just superior to the target, deflection may occur when the electrode is extended from this point for tissue exploration. Although little has been published on this topic, we are aware of one study that addresses it. Dr. G. Heit, Department of Neurosurgery at the Stanford Brain Research Center, characterized the extent of probe deflection from a sample of 252 microelectrode tracks using registered orthogonal X-rays (personal communication). The deflection observed in this sample was on average 0.5 mm at the tip. As our participating hospitals do not incorporate this X-ray-based measurement technique, this source of error in our data cannot be quantified.

It is impossible to account for alteration of stimulation-induced experiential effects or modulation of neuronal spike trains by drugs administered to the patient before surgery that act on the central nervous system. While our collaborating surgeons tend to perform this surgery with the patient un-medicated, there were times when this was not possible. Patients with severe Parkinsonism, for example, occasionally require reduced quantities of medications to permit articulation of limbs or facilitate speech during the procedure.

Most patients experience very little brain shift resulting from cerebrospinal fluid loss out the burr hole and it is not a major cause for concern. However, elderly patients with larger ventricles or extensive cortical atrophy may experience larger deformations of the cortex, sometimes up to 9 mm [34], during open stereotactic surgery. As a result, these patients will generate functional data that, once tagged to their preoperative MR image, have the potential to become progressively more misregistered with the insertion of each subsequent trajectory. Linear registration of a postoperative MR image to the preoperative image is the only way to quantifiably assess the extent of brain shift that has compounded throughout the procedure. This image-based approach provides no information regarding the rate of shift and thus, to confidently remove any potential effects of brain shift from patients whose target anatomy exhibits shift, we must discard all functional data other than those derived from the first exploratory trajectory. This first trajectory, we can safely assume, is the least affected by shifting of brain geometry. We are currently examining the postoperative MRIs of every patient who has contributed data to the functional database so potentially contaminated data can be removed.

V. Conclusion

The ASP system has been used intraoperatively for plotting and analyzing functional data in patient preoperative image space during five separate surgeries. Although the database was not at a stage of development where prediction of surgical targets was possible, the visualization capabilities designed for presentation of database contents nevertheless proved useful intraoperatively. In conjunction with the ability of the ASP system to automatically calculate frame-to-MRI transforms, model trajectories at appropriate frame coordinates, and

display electrophysiologic data as discreet 3-D objects, the patient data were coded and plotted directly onto trajectories mimicking the actual probe tract as they were produced. The use of ASP to immediately incorporate patient responses into the patient's 3-D MR image is a substantial improvement over the method used here and elsewhere, where trajectories and electrophysiologic data are labeled onto an overhead projection of a photocopied series of the Schaltenbrand Wahren atlas. Intraoperative annotation of the patient MRIs did not extend the normal duration of the procedure.

These efforts have laid the groundwork for a database of functional organization of subcortical anatomy explored during stereotactic neurosurgery. We have described a system capable of storing and retrieving population electrophysiology without the use of anatomical atlases or AC–PC-based scaling techniques and described how it may be applied to frame-based image-guided stereotaxy. A digital probabilistic atlas of this nature that utilizes population data will improve in accuracy over time and achieve better statistics upon the addition of more patient data. While only qualitative results were presented in this paper, with 106 procedures currently in the database providing over 10 000 data points, we are now in a position to commence validation studies that quantitatively assess its predictive abilities.

ACKNOWLEDGMENT

The authors would like to thank Dr. C. Holmes for the use of the standard reference MR brain volume and Mr. D. G. Gobbi of The John P. Robarts Research Institute, for his technical assistance, his computer advice, and his software contributions to modules used in this project and to the VTK repository in general.

REFERENCES

[1] G. Schaltenbrand and W. Wahren, *Atlas for Stereotaxy of the Human Brain*. Stuttgart, Germany: Thieme, 1977.

[2] J. van Buren and R. Borke, *Variations and Connections of the Human Thalamus*. Berlin, Germany: Springer, 1972.

[3] W. L. Nowinski, T. T. Yeo, and G. L. Yang, "Atlas-based system for functional neurosurgery," in *Proc. SPIE Medical Imaging*. Bellingham, WA: SPIE, 1997, vol. 3031, Image Display, pp. 92–103.

[4] G. Bertrand, A. Olivier, and C. J. Thompson, "The computerized brain atlas: Its use in stereotaxic surgery," *Trans. Amer. Neurological Assoc.*, vol. 98, pp. 233–237, 1973.

[5] P. M. Thompson and A. W. Toga, "Warping strategies for intersubject registration," in *Handbook of Medical Imaging*, W. Brody and E. Zerhouni, Eds. San Diego, CA: Academic, 2000, pp. 659–601.

[6] B. A. Kall, P. J. Kelly, S. J. Goerss, and G. Frieder, "Methodology and clinical experience with computed tomography and a computer-resident stereotactic atlas," *Neurosurgery*, vol. 17, no. 3, pp. 400–407, 1985.

[7] P. St-Jean, A. F. Sadikot, D. L. Collins, D. Clonda, R. Kasrai, A. C. Evans, and T. M. Peters, "Automated atlas integration and interactive 3-dimensional visualization tools for planning and guidance in functional neurosurgery," *IEEE Trans. Med. Imag.*, vol. 17, pp. 672–680, Oct. 1998.

[8] R. M. Lehman, J. Zheng, J. L. Hamilton, and E. Micheli-Tzanakou, "Comparison of 3-D stereoscopic MR imaging with pre and post lesion recording in pallidotomy," *Acta Neurochir. (Wein)*, vol. 142, pp. 319–328, 2000.

[9] D. L. Collins, C. J. Holmes, T. M. Peters, and A. C. Evans, "Automatic 3-D model-based neuroanatomical segmentation," *Human Brain Map.*, vol. 3, pp. 190–208, 1995.

[10] J. Talairach and P. Tourneau, *Co-Planar Stereotaxic Atlas of the Human Brain*. Stuttgart, Germany: Georg Thieme Verlag, 1988.

[11] F. Afshar, E. S. Watkins, and J. C. Yap, *Stereotactic Atlas of the Human Brainstem and Cerebellar Nuclei. A Variability Study*. New York: Raven, 1978.

[12] V. H. Mark and P. L. Yakovlev, "A note on problems and methods in the preparation of a human stereotactic atlas," *Anat. Rec.*, vol. 121, pp. 745–752, 1995.

[13] W. L. Nowinski, A. Fang, B. T. Nguyen, J. K. Raphel, L. Jagannathan, R. Raghavan, R. N. Bryan, and G. A. Miller, "Multiple brain atlas database and atlas-based neuroimaging system," *Comput. Aided Surg.*, vol. 2, pp. 42–66, 1998.

[14] M. Yoshida, "Creation of a three-dimensional atlas by interpolation from Schaltenbrand–Bailey's atlas," *Appl. Neurophysiol.*, vol. 50, pp. 45–48, 1987.

[15] J. Guridi, A. Gorospe, E. Ramos, G. Linazasoro, M. C. Rodriguez, and J. A. Obeso, "Stereotactic targeting of the globus pallidus internus in Parkinson's disease: Imaging versus electrophysiological mapping," *Neurosurgery*, vol. 45, no. 2, pp. 278–287, 1999.

[16] R. L. Alterman, D. Sterio, A. Beric, and P. J. Kelly, "Microelectrode recording during posteroventral pallidotomy: Impact on target selection and complications," *Neurosurgery*, vol. 44, pp. 315–321, 1999.

[17] P. A. Starr, J. L. Vitek, M. DeLong, and R. A. Bakay, "Magnetic resonance imaging-based stereotactic localization of the globus pallidus and subthalamic nucleus," *Neurosurgery*, vol. 44, no. 2, pp. 303–313, Feb. 1999.

[18] M. Zonenshayn, A. R. Rezai, A. Y. Mogilner, A. Beric, D. Sterio, and P. J. Kelly, "Comparison of anatomic and neurophysiological methods for subthalamic nucleus targeting," *Neurosurgery*, vol. 47, no. 2, pp. 282–292, 2000.

[19] C. J. Thompson, T. L. Hardy, and G. Bertrand, "A system for anatomical and functional mapping of the human thalamus," *Comput. Biomed. Res.*, vol. 10, pp. 9–24, 1977.

[20] R. R. Tasker, L. W. Organ, and P. A. Hawrylyshyn, *The Thalamus and Midbrain of Man*. Springfield, IL: Charles C. Thomas, 1982.

[21] C. Giorgi, U. Cerchiari, G. Broggi, P. Birk, and A. Struppeler, "Digital image processing to handle neuroanatomical information and neurophysiological data," *Appl. Neurophysiol.*, vol. 48, pp. 30–33, 1985.

[22] M. Yoshida, K. Okada, A. Nagase, S. Kuga, M. Shirahama, M. Watanabe, and S. Kuramoto, "Neurophysiological atlas of the human thalamus and adjacent structures. Computer-assisted mapping," *Appl. Neurophysiol.*, vol. 45, pp. 406–409, 1982.

[23] G. Bertrand, J. Blundell, and R. Musella, *Electrical Stimulation of the Internal Capsule and Neighboring Structures During Stereotactic Procedures*. Philadelphia, PA: Harvey Cushing Soc., Apr. 20, 1963.

[24] G. Schaltenbrand and P. Bailey, *Introduction to Stereotaxis With an Atlas of the Human Brain*. Baltimore, MD: Williams and Wilkins, 1959.

[25] Y. P. Starreveld, D. G. Gobbi, K. W. Finnis, and T. M. Peters, "Software components for medical image visualization and surgical planning," in *Proc. SPIE Medical Imaging*. Bellingham, WA: SPIE, 2001, vol. 4319, Visualization, Display and Image-Guided Procedures, pp. 546–556.

[26] J. B. Ranck, Jr., "Which elements are excited in electrical stimulation of mammalian central nervous system: A review," *Brain Res.*, vol. 98, pp. 417–440, 1975.

[27] D. L. Collins and A. C. Evans, "ANIMAL: Validation and applications of nonlinear registration-based segmentation," *Int. J. Pattern Recogn. Artif. Intell.*, vol. 11, no. 8, pp. 1271–1294, 1997.

[28] Y. P. Starreveld, "Fast nonlinear registration applied to stereotactic functional neurosurgery," Ph.D. dissertation, Univ. Western Ontario, London, ON, Canada, June 2002.

[29] C. J. Holmes, R. Hoge, D. L. Collins, R. Woods, A. W. Toga, and A. C. Evans, "Enhancement of MR images using registration for signal averaging," *J. Comput. Assist. Tomogr.*, vol. 22, no. 2, pp. 324–333, 1998.

[30] P. Kochunov, J. L. Lancaster, P. Thompson, R. Woods, J. Mazziotta, J. Hardies, and P. Fox, "Regional spatial normalization: toward an optimal target," *J. Comput. Assist. Tomogr.*, vol. 25, no. 5, pp. 805–816, Sept. 2001.

[31] M. C. Rodriguez, J. A. Obeso, and C. W. Olanow, "Subthalamic nucleus-mediated excitotoxicity in Parkinson's Disease: A target for neuroprotection," *Ann. Neurol.*, vol. 44, no. 3, Suppl. 1, pp. 175–188, 1998.

[32] D. Sterio, M. Zonenshayn, A. Mogilner, A. R. Rezai, K. Kiprovski, P. J. Kelly, and A. Beric, "Neurophysiological refinement of subthalamic nucleus targeting," *Neurosurgery*, vol. 50, pp. 58–67, 2002.

[33] G. Bertrand, A. Olivier, and C. J. Thompson, "Computer display of stereotaxic brain maps and probe tracts," *Acta Neurochir. (Wien)*, pp. 235–243, 1974.

[34] K. Wester and J. Krakenes, "Vertical displacement of the brain and the target area during open stereotactic neurosurgery," *Acta Neurochir.*, vol. 143, pp. 603–606, 2001.